

Article

Not peer-reviewed version

---

# Development of Novel Hydraulic 3D Printed Actuator Using Electrorheological Fluid for Robotic Endoscopy

---

[Fabian Sadi](#)\*, Jan Holthausen, Jan Stallkamp, Marius Siegfarth

Posted Date: 27 February 2024

doi: 10.20944/preprints202402.1526.v1

Keywords: electrorheological actuator; 3D printing; snake-like endoscopic robot; hydraulic actuation; miniaturized actuator design




Preprints.org is a free multidiscipline platform providing preprint service that is dedicated to making early versions of research outputs permanently available and citable. Preprints posted at Preprints.org appear in Web of Science, Crossref, Google Scholar, Scilit, Europe PMC.

Copyright: This is an open access article distributed under the Creative Commons Attribution License which permits unrestricted use, distribution, and reproduction in any medium, provided the original work is properly cited.

## Article

# Development of Novel Hydraulic 3D Printed Actuator Using Electrorheological Fluid for Robotic Endoscopy

Fabian Sadi \* , Jan Holthausen, Jan Stallkamp and Marius Siegfarth

Mannheim Institute of Intelligent Systems in Medicine, Ruprecht-Karls University Heidelberg, 68167 Mannheim, Germany

\* Correspondence: fabian.sadi@medma.uni-heidelberg.de; Tel.: +49 (0)621 383-8525

**Abstract:** Endoscopy has made a significant and noteworthy contribution to the field of medical science and technology. Nevertheless, its potential remains constrained due to the limited availability of rigid or flexible endoscopes. This paper introduces a novel hydraulic actuator based on electrorheological fluid (ERF) as a pivotal advancement in bridging the existing gap within the realm of endoscopy. Following a comprehensive introduction that briefly outlines the electrorheological effect, the subsequent section is dedicated to the elucidation of the actuator's development process. Challenges arise, particularly in terms of miniaturization and the realization of a hydraulically sealed system with integrated valve electrodes. An internal electrorheological valve system consisting of four valves that are controlled using a pulse-width modulated high voltage was suitable for position control of the antagonistic hydraulic actuators. High-precision stereolithography (SLA) printing has proven practical for manufacturing the actuator components. For functional testing, a test bench was set up in which the actuator follows a setpoint through a PI control loop. The control deviation ranged from 0.6 to 1 degree, with a response time between 6 and 8 seconds. The experiments have demonstrated that, through the use of ERF and integrated valve electrodes, a miniaturized functional actuator can be constructed.

**Keywords:** electrorheological actuator; 3D printing; snake-like robot, medical robotics, hydraulic actuation

## 1. Introduction

Minimally invasive surgical procedures have revolutionized the field of medicine, enabling faster patient recovery and reduced post-operative complications. Currently, either rigid or flexible endoscopes that are available on the market are used, depending on the requirements of the procedure. Flexible systems achieve excellent maneuverability; however, due to their flexibility, they struggle to effectively withstand forces during operative procedures. Conversely, rigid endoscopes can provide better stability, but significantly limit access possibilities. In this work, we present a novel hydraulic actuator module based on Electrorheological Fluid. This module will serve as the propulsion unit for a snake-like robotic endoscope, ensuring both structural rigidity and flexibility (Figure 1). The development of a modular design with integrated, leak-free valve electronics significantly contributes to the advancement of hydraulically actuated medical robotics..

### 1.1. Actuation concept

The actuator is operated using an electrorheological fluid (ERF), which falls into the category of smart fluids. The fluid itself is a suspension containing a carrier liquid (often silicone oil) with electrically polarizable particles (e.g., titanium dioxide) [1]. Within this fluid, the yield stress can be selectively increased reversibly by applying an electrical voltage across two electrodes, generating an electric field. According to [2], the ERF's flow curve can be described using the Bingham model, with shear stress  $\tau$ , yield stress  $\tau_0$  which depends on the electric field strength  $E$ , viscosity  $\eta$  and shear rate  $\dot{\gamma}$ :

$$\tau = \tau_0(E) + \eta\dot{\gamma} \quad (1)$$

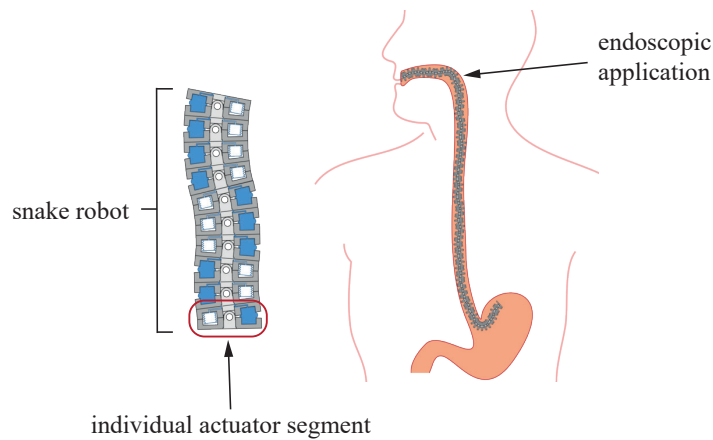


**Figure 1.** Schematic representation of the hydraulic snake-like robot for endoscopic application

The electrorheological effect in a hydraulic channel is depicted in Figure 2. Within milliseconds, dipoles are induced in the solid particles, resulting in an electric torque. Consequently, the particles align along the field lines, forming mechanically loadable chains [2]. The fluid consequently solidifies into a plastic-like substance, retaining this state up to a yield stress of  $\tau_0$ . Beyond  $\tau_0$ , the chains disintegrate, enabling the fluid to flow once again. By switching an electric voltage, this behaviour can be intentionally induced, rendering it suitable for use as a valve. The parameters for sizing the valve, according to [3], include the volumetric flow rate  $Q_p$ , the yield stress of the fluid  $\tau_0$  dependent on the electric field  $E$ , and the maximum pressure to be switched, i.e., the pressure difference  $\Delta P_p$ .

$$\Delta P_p = 12\eta \frac{L}{h^3b} Q_p + 2\frac{L}{h} \tau_0(E) \quad (2)$$

with viscosity  $\eta$ , channel height  $h$ , channel width  $b$ , and channel length  $L$ . The pressure difference consists of the component attributed to the intrinsic viscosity of the fluid and the pressure difference that can be activated by the electro-rheological effect. In designing the channel geometry, attention should be paid to not choosing the channel height excessively high, particularly in accordance with Equation (2), to minimize the geometric influence.

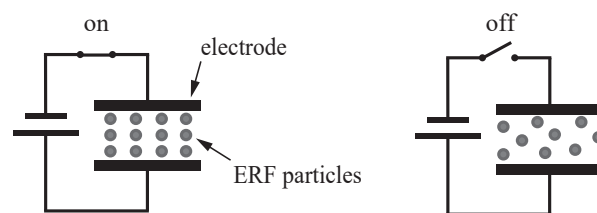


**Figure 2.** Use of the ER effect for a hydraulic valve. On the left, with high voltage applied. ERF particles align along the electric field lines and form mechanically stable chains. On the right, without high voltage. The ERF particles flow through the channel

The use of an electrorheological fluid for hydraulic actuation brings about two significant advantages. Firstly, ERF offer an excellent possibility for miniaturization by eliminating the need for mechanically moving valve components. Secondly, hydraulics provide high power density, ensuring that even in miniaturized actuators, the driving forces remain high [4]. Hydraulic actuators are particularly well-suited for actuating soft robots that allow for safe interaction with humans [5]. At the same time, they can be stiffened, creating an ideal platform for manipulations. Regarding applications

in medical robots, hydraulic actuators do not require ferromagnetic components, which is crucial for applications in magnetic resonance imaging (MRI) environments to reduce the risk of artifact generation [6]. Fast response times as well as the easy control of valves via thin high-voltage wires also make the use of ERF appealing. Here, we present a novel integrated valve concept for controlling a 3D printed and miniaturized actuator module for application in endoscopy. Our contributions are:

1. Development of a suitable manufacturing process for a miniaturized and pressure-tight ERF hydraulics.
2. Integration of a suitable sensor for measuring the actuator rotation.
3. Establishment of a control system to maneuver the actuator module to a desired position.

Hydraulic actuator constructions often consist of two or more bellows mounted between two platforms. The pressure variation in the individual bellows and an appropriate cascading of the actuator modules enable multi-directional bending and elongation with a variable stiffness of the snake robot. This is demonstrated, among other, in research works by [4,7–9].

In the domain of minimally invasive surgery, well-established actuation techniques for soft snake robot concepts have garnered significant attention. These techniques encompass fluid-driven, cable-driven, and electromagnetic-driven methodologies [10]. Specifically focusing on fluid-driven concepts, the spatial constraints posed by endoscopic actuators often necessitate the external placement of conventional fluid valves. Consequently, the sequential interconnection of actuator segments is frequently confined to a mere two or, at most, three actuators due to the increasing proliferation of input and output connections for each actuator segment [11]. The potential for miniaturization is notably heightened in cable- and wire-driven actuators, wherein slender cables traverse multiple actuator segments. However, this advantage comes at the cost of heightened frictional losses. It is pertinent to note that within this context, the cable-driven mechanism remains positioned externally to the snake robot, demanding a substantially more intricate design and control effort [12]. Electromagnetic drive modules necessitate intricate apparatus to sustain a stable magnetic field for the facilitation of motion control. Additionally, the ability to assume intermediary positions is not feasible, resulting in a curtailed range of motion. Nonetheless, electromagnetic actuators can be miniaturized down to the millimeter scale [10]. The application of ERF in robotic systems is not very widespread. They have primarily been used for the implementation of active dampers and couplings [13,14]. However, there are also works that demonstrate their use in soft robotics [15,16]. The valve presented in [15] even illustrates the possibility of manufacturing ER valves directly through 3D printing. The presented valve design features electrodes that do not come into direct contact with the ERF. However, with this external electrode arrangement, we were unable to manipulate our ERF. Therefore, a design with electrodes in direct contact was pursued.

## 2. Materials and Methods

The application in endoscopy requires an exceptionally space-efficient actuator design. The endoscopic application is limited to oral access because, in the initial stages, it is technically easier to implement due to less torsion of the endoscope. The esophagus of an adult human has a diameter of approximately 20 mm, which is why gastroscopes often have an overall diameter of 5-10 mm [17]. The technical challenges within these size ratios are immense, which is why, in the initial actuator concept, we aimed for an overall diameter of 20 mm. Subsequent developments should build upon this concept to achieve further miniaturization. The developed single actuator configuration is depicted in Figure 3. The bellows are designed using a semi-circular geometry with a maximized surface area to maintain actuator force even at lower hydraulic pressures. The actuator assembly is composed of a sandwich structure consisting of individual 3D printed modules. These modules serve two primary functions: forming the valve body itself and connecting the antagonistic bellows to one another through a pivot joint (Figure 3).

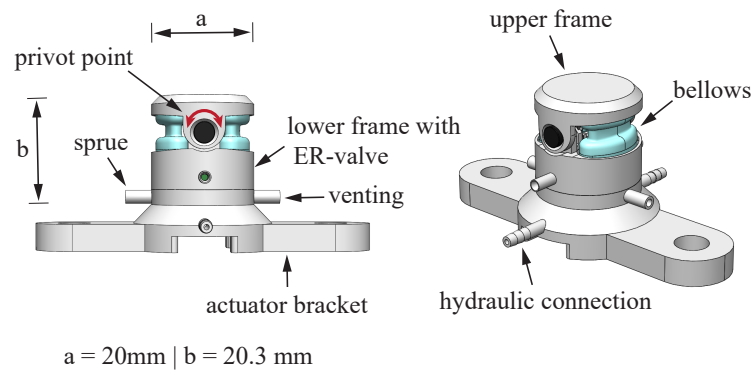


**Figure 3.** ER actuator CAD design: On the left, there is a side view with dimensions for the actuator’s width and height, as well as a sprue and venting for the valve manufacturing process. On the right, 3D representation of the actuator module.

As elucidated in section 1, an ER valve necessitates the presence of two opposing electrodes to modulate the yield stress of the ERF via the application of an electric field. Collectively, each actuator module requires four valves to facilitate the implementation of inlet and outlet channels for the two bellows. Figure 4 illustrates the structure of the microvalve. To achieve space-efficient integration of the four valve electrodes, two PCBs (Printed Circuit Boards) were designed using the open-source software KiCad. Within the valve body, these two PCBs are spatially stacked on top of each other (Figure 4 right). The upper PCB is divided into four segments at the valve locations. The lower PCB functions as the counter electrode and is designed as a simple ring. The valve concept becomes evident when examining Figure 4 on the left side and superimposing the two PCBs. In this scenario, two opposing segments of the valve on the upper PCB are connected to the voltage source. The ring electrode serves as the electrical ground. This arrangement facilitates the transfer of the ERF from the hydraulic pressure side to the first bellows connection. Simultaneously, the valve segment of the second bellows connection is open, allowing the ERF to flow from the second bellows into the drain, resulting in an actuator tilting motion. To return the actuator to its initial position or to tilt it in the opposite direction, the ring electrode is connected to the voltage source, while the other two opposing valve segments act as electrical grounds.

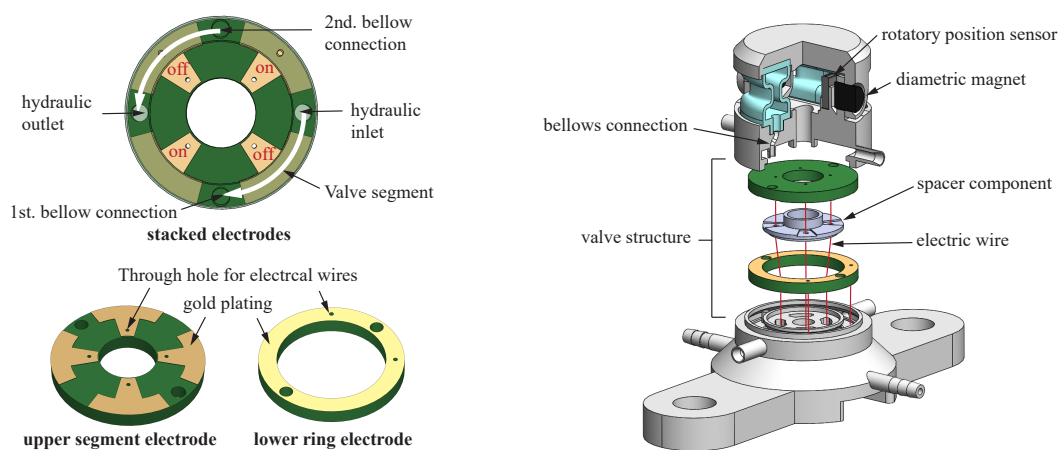


**Figure 4.** ER valve structure. On the left, PCB design of the lower ring electrode and upper segment electrode. Stacked electrode view, demonstrating the valve logic using a circuit example. On the right, exploded view of the ER valve assembly.

To control the actuator for different tilt angle positions and directions, it is necessary to integrate a sensor that can detect and reproduce these movements. The tilt angle range is  $\pm 20$  degrees per side, resulting in a total excursion of the actuator of 40 degrees. The contactless rotational angle sensor

AS5600 (ams-OSRAM AG, Austria) has been utilized for a precise and easily miniaturizable angular measurement. This sensor measures the absolute angle of a diametrically magnetized permanent magnet rotating on the vertical axis with respect to the sensor. The magnet is directly integrated as a pivot pin into the upper half of the frame, as shown in Figure 4 right. The sensor covers an angle range from 18 to 360 degrees. Through the integrated I<sup>2</sup>C interface, the sensor's gain is programmed based on the actuator's angular deflection, thus enhancing accuracy. For the overall assembly of the snake robot from individual actuator modules, a concept has been developed to facilitate hydraulic pressure supply through a central high-pressure and low-pressure line. However, for the subsequent experiments, initially, only a single actuator module will be assembled and tested. The arrangement of the actuator modules is illustrated in Figure 5a. Each actuator module is positioned with a 90-degree offset to achieve the snake-like motion.

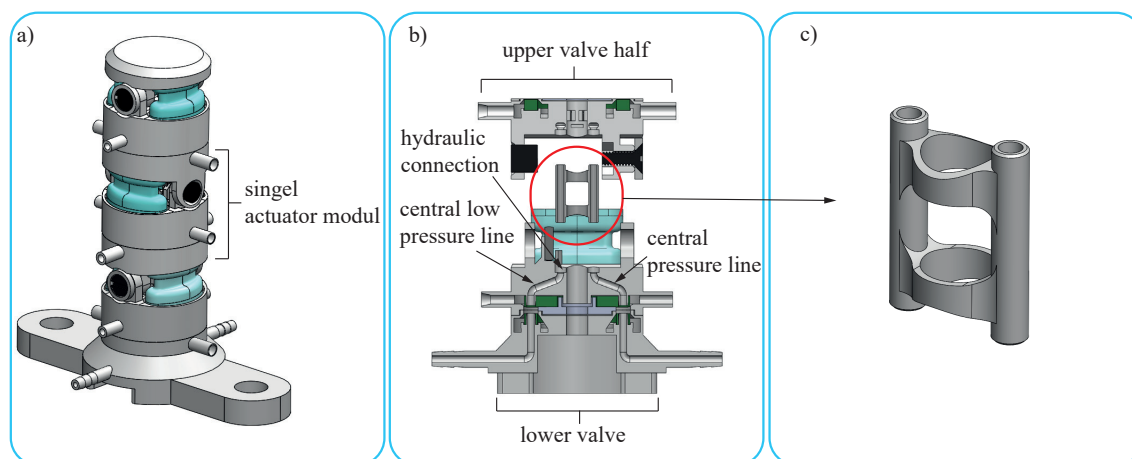


**Figure 5.** Construction of the snake-like robot with a central hydraulic connection to the individual actuator modules. a) snake-like robot constriction b) Sectional view of an actuator module with a central pressure line and a connector to the next actuator module. The upper frame simultaneously represents the lower valve half of the next actuator. c) Hydraulic connector with two channels for high-pressure and low-pressure connections.

The sectional view in Figure 5b illustrates the central hydraulic lines for the high-pressure and low-pressure channels. The connection between the bellows must be made of a flexible material to prevent collisions due to the tilting motion of the upper frame half of the actuator. Due to the limited space, the inner diameter of the individual channel is only 1 mm, with a wall thickness of 0.5 mm. For a simplified assembly of the slender connecting hoses, they are linked together using ring segments at both the top and bottom (see Figure 5c). Specific inserts for the upper and lower ring segments are provided at their respective connection points. This facilitates easy insertion from both the top and bottom during the assembly process.

## 2.1. Materials and Methods

### 2.1.1. Actuator fabrication

For the fabrication of a miniaturized hydraulic actuator utilizing electrorheological fluid, various manufacturing processes were considered. The foremost challenge within the manufacturing process lies in ensuring a compact and enclosed construction that amalgamates diverse material rigidities. Additionally, the valve electrodes must be directly inserted into the hydraulic channel. Initial deliberations focused on casting methods utilizing a core of fusible wax. 3D printed negative molds of the actuator hydraulics were developed for this purpose, facilitating the creation of wax molds. Valve electrodes were then placed onto the wax negative molds. Subsequently, the wax negative molds, along with the electrodes, were subjected to silicone dip molding. Ultimately, the liquid

wax altered the material properties of the silicone during the debinding process, rendering it prone to cracking and brittleness. Consequently, this manufacturing process did not yield satisfactory outcomes. A conventional manufacturing approach for producing intricate geometries is 3D printing. Certain 3D printing technologies, such as Fused Deposition Modeling (FDM) or Multi Material Jetting (MMJ), even enable pause printing at a desired height, allowing for the insertion of components or electrical elements. Nonetheless, FDM methods suffer from the drawback of limited precision, thereby potentially leading to faster hydraulic component leakages. The precision constraints further complicate the production of miniaturized components [18]. MMJ printing technologies, on the other hand, are significantly more precise and also enable the production of small-scale components with varying material stiffness. However, the material properties of MMJ-technologies are often brittle and light-sensitive, making flexible materials more prone to leakage [19]. The high costs of these 3D printers, as well as the labor-intensive post-processing associated with this technology, further limit the use of this manufacturing method. Stereolithography (SLA), a 3D printing technology that employs UV laser-assisted layer curing, facilitates the production of highly intricate and small components with a high degree of accuracy. The flexible material Elastic 50A (Formlabs, USA) is capable of withstanding multiple load cycles, further emphasizing the advantages of SLA printing technology [20]. However, a drawback of this manufacturing process is the limitation to print with only a single material during the printing process. During the printing process, it is not possible to insert and integrate components into the printed parts, as the printed parts immerse into a bath of 3D printing resin with each layer. As a result, components must subsequently be assembled in a modular fashion. Nonetheless, a modular assembly of the actuator necessitates a pressure-tight connection of individual parts, which is developed and presented herein. Adhesive connections, such as with instant glue or multi-purpose adhesive, do not lead to reliably sealed connections, as the adhesives are often rigid and lose their adhesive strength after a certain period of time. Especially with flexible materials that exhibit low surface energy, adhesive forces can mostly be established through prior surface treatments [21,22]. The developed assembly connection thus consists of an assembly process using flexible (SLA) 3D printing material, which is injected as a liquid into the components and subsequently cured under UV light. For this purpose, channels were introduced into the 3D printed valve halves and provided with a sprue and a vent (Figure 6). The sprue and vent can be easily removed with pliers after the manufacturing process.

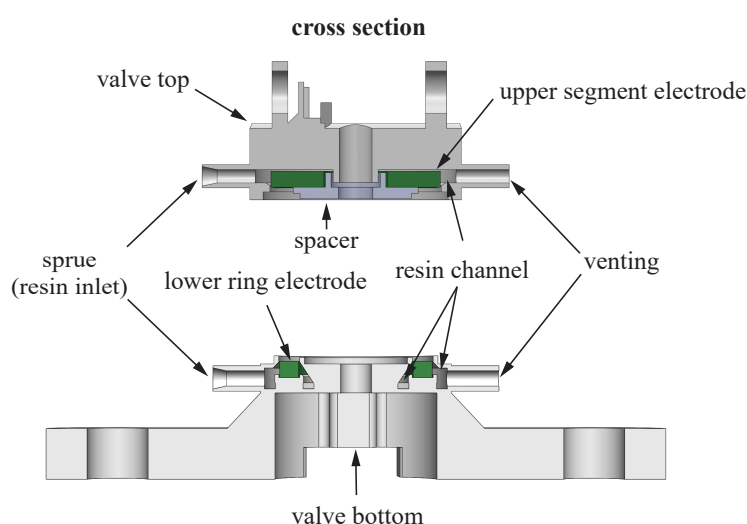


**Figure 6.** 3D-printed valve halves with channels for casting the electrodes. On the top, the upper valve half with the segment electrode. On the bottom, the lower valve half with the ring electrode.

Through this manufacturing process, the PCB electrodes are encapsulated into the respective valve half and pressure-tightly connected to the 3D printed body. Elastic 50A was used as a flexible

3D printing material for bonding and sealing. This material exhibits similar material properties to silicone with the same Shore hardness [20]. The valve halves are made of formlabs Clear, which possesses transparent material properties and is thereby UV transmissive. The connection wires of the electrodes are guided outward through a central channel (Figure 4 right). As a result, the segments of the upper electrode were designed in a T-shape to the interior (Figure 4 left) to allow the wires to pass by the lower ring electrode. In order to define the channel width of the segment electrode, an spacer was constructed (Figure 6). The connection of the spacer is achieved by applying the SLA material Elastic 50A and curing it under UV light. In the next step, the two valve halves are assembled. The contact surfaces are coated once again with Elastic 50A and then the entire valve body is cured under UV light. The connection of the bellows to the upper and lower frame halves follows the same manufacturing process. However, before bellows assembly, the rotary angle sensor (AS5600) is inserted. The sensor cables are also threaded through the channel in the center of the actuator. The joint design and the assembly method at the bellows ensure that the bellows can be relatively easily replaced. This is of significant advantage in case of bellows failure.

### 3. Experiments

#### 3.0.1. Experiment setup

The actuator was integrated into a test bench, shown in Figure 8a, where the hydraulic inlet was connected to a syringe filled with electrorheological fluid. The fluid consisted of Titanium dioxide nanoparticles and silicone oil (GER STD 0201, Smart Materials Laboratory, Hong Kong).

The initial experiments demonstrating the behavior of the fluid in a valve circuit were presented in [3], which is why not explicit attention is given to it again here. A constant fluid pressure was achieved by connecting the syringe to pressure-controlled compressed air. The arrangement of the ER-valves as a hydraulic bridge circuit is illustrated in Figure 7, with the outer electrodes representing the upper segment electrode and the inner electrodes being the ring electrode. The opposite segments of the upper electrode were connected to the negative and positive poles of a 5 kV high voltage source (Ultravolt 5HVA24-BP1, Advanced Energy, USA) as shown in Figure 7. To control the voltage of the lower ring electrode, high voltage optocouplers were used, thus making it possible to switch the voltage of the ring electrode between the high and low level. The optocouplers and position sensor were connected to a data acquisition system to enable control using a computer running Simulink. The duty cycle of a 100 Hz pulse width modulated signal was used to achieve analog control of the valves. For controlling the actuator in Simulink, a PID block was utilized, although it was employed as a PI-controller only. The target angle was given as the input and the deviation between the target angle and actual angle obtained from the rotational sensor was used as the controller input. The controller then calculates an appropriate duty cycle value between 0 and 1. The adjustment of the control parameters was done by manually tuning the P and I terms based on the system's step response. The determined P and I terms can be seen in Figure 8d).

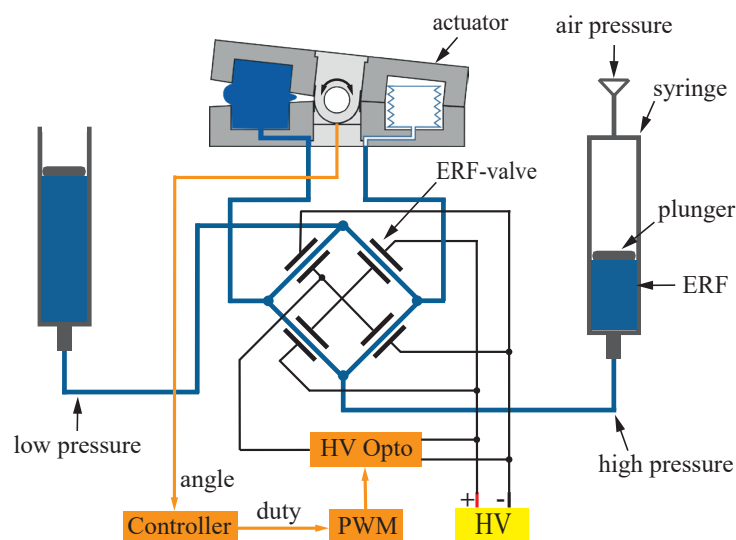


**Figure 7.** Block diagram of the test bench setup of the ERF actuator, including hydraulic and electrical schematics.

#### 4. Results

The functioning of the PI control of the actuator was examined using a target angle profile (Figure 8e, orange curve). The actuator deflection was set to 10 degrees in both the positive and negative directions, corresponding to half of the maximum tilt angle of 20 degrees. After reaching the setpoint, it was held for a duration of 35 seconds to observe the settling behavior. During this time, an overshoot of up to 1 degree was observed for the initial three target angle increments. However, the measurement curve gradually approached the setpoint over time. With a longer simulation duration, the setpoint could potentially be reached. Nevertheless, the possible simulation duration was reduced by the limited number of cycles the 3D-printed bellows were able to withstand. Due to frequent expansion and compression of the bellows, failure occurred after approximately 10-15 cycles, causing the bellows to rupture. In Figure 8e, the failure of a bellows can be observed, which occurred when the target position was changed from -10 degrees to 0 degrees. Due to the sudden pressure release, the measurement signal significantly exceeds the setpoint to 2.6 degree (Figure 8e, blue curve). The response time of the actuator primarily depends on the controller parameters, with a significant influence from the pump pressure. Increased pump pressure allows the ER fluid to flow more rapidly through the channels into the bellows, improving the actuator's ability to track the setpoint. To achieve an appropriate response time for the controller settings and the experimental procedure, an evaluation of the pump pressure had to be conducted, keeping it within the bellows expected lifespan. Consequently, the pump pressure was gradually increased to 2.4 bar. At this pump pressure, response times between 6 and 8 seconds were measured. The final actuator return to the zero position cannot be considered due to bellows failure.

The silicone-like photopolymer material Elastic 50A undergoes a rapid aging process. After two to three days following the printing and curing process (Formlabs Form Cure, 60 degrees for 20 minutes), the material properties became brittle, resulting in a faster material failure. An accelerated aging process was observed when the 3D printed bellows were exposed to natural UV radiation. Additionally, the 3D printing process itself results in a weakening of the components due to the layer-by-layer material deposition, which can be avoided through casting processes. Silicone-cast bellows would be expected to provide better long-term stability due to the closed material layer, thereby enabling longer testing periods. This would significantly enhance the characterisation of the actuator, as tuning of the controller must be adjusted with each bellows replacement. Simultaneously, higher system pressures are allowed, improving response times during control operation. However,

the bonding method developed here shows significant potential. In the experiments, there were no leakages at any of the connection points. It is noteworthy that this manufacturing method reliably realizes very small channels (channel height: 1 mm and channel width: 2.2 mm) while integrating valve electronics.

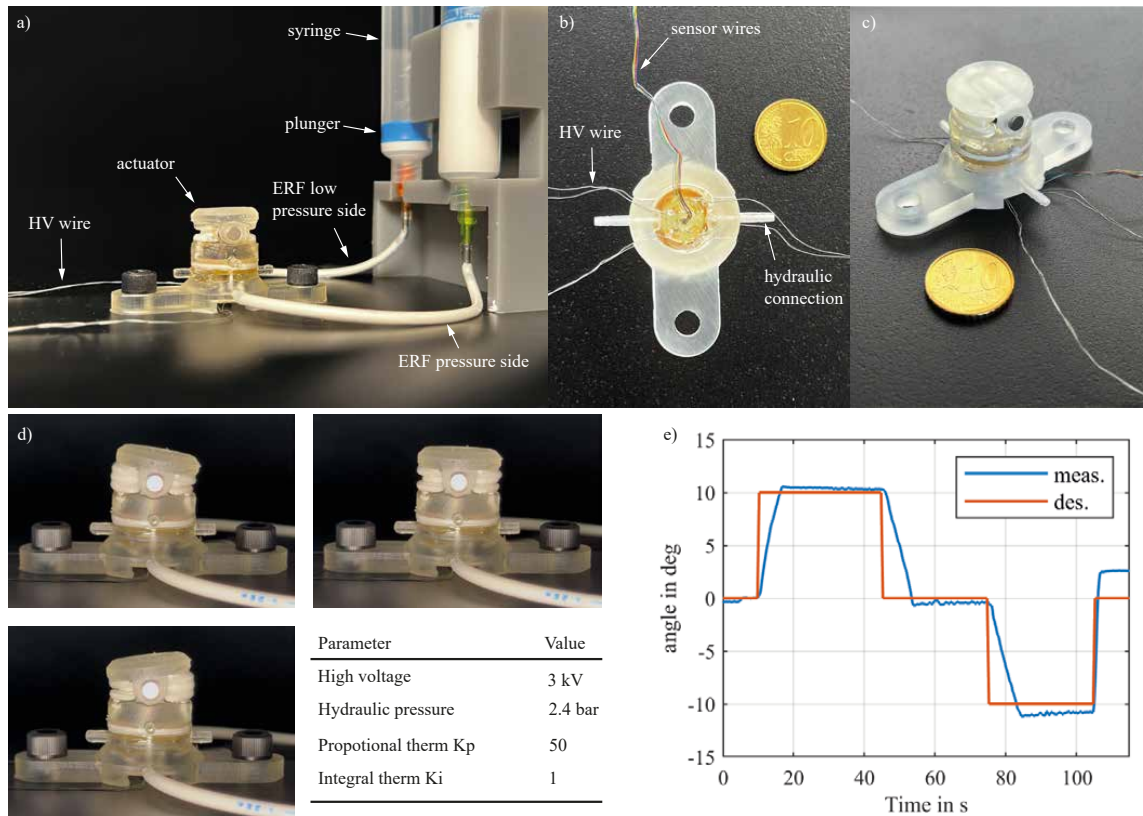


**Figure 8.** Experimental setup for actuator functional test. a) A syringe filled with ERF was connected to both the pneumatic pressure side and the hydraulic connection of the actuator. On the other hydraulic connection of the actuator, an empty syringe was connected. The HV cables and sensor cables were connected to the high-voltage source, HV optocouplers, and to the I/O of the data acquisition box. b) Bottom view of the actuator with sensor and high-voltage wire routing through the center of the actuator. c) Perspective view of the actuator with representation of scale using a 10 cent coin. d) Tilting motion and the neutral position of the actuator, in dependence on the PI control curve, along with the testing parameters for the experimental procedure. e) PI controller diagram plotted with degrees over time. The setpoint curve is shown in orange, featuring a 10 degree tilt of the actuator in the positive direction, a neutral position, and a 10 degree tilt in the negative direction. Dwell times per position step were 35 seconds. The blue curve represents the controlled actuator trajectory. Rupture of one bellow occurred at 105 s.

5. Discussion

This work presents the development of a miniaturized hydraulic tilting actuator as part of a robotic endoscope, based on electrorheological fluid. By utilizing precise SLA 3D printing technology and a developed assembly technique for the components, it was possible to create a hydraulically sealed 3D printed actuator with integrated valves and a sensor. The encapsulation of the electrodes with the 3D printing material Elastic 50A proved to be the most effective solution. Component irregularities and tolerances, which significantly contributed to system leakage, were easily compensated for. The advancements in this development constitute a significant contribution to the implementation of hydraulically sealed actuation systems in medical robotics. Due to the sterility requirements in medicine, any leakage is not tolerated [23]. The use of electrorheological fluid allows for the development of highly miniaturized valves to be integrated into the robotic system. Simultaneously, the nearly

incompressible properties of hydraulic actuation provide a high power density, which is essential for effective miniaturization [24]. Additional development work would be needed for endoscopic application to achieve a maximum outer diameter of up to 10 mm.

The functionality of the tilting actuator was demonstrated through PI control in bench tests with an accuracy of 0.6 to 1 degree and response times between 6 and 8 seconds. The proposed electrorheological valve system consisting of four valves that are controlled using a single high voltage PWM signal proved suitable for the control of the two antagonistic actuators. However, functional tests also revealed weaknesses in the 3D printed bellows. Extensive testing including system identification and controller tuning was not possible using the current test setup. Future work must therefore focus on more stable and durable hydraulic bellows that can withstand higher pressure and more movement cycles. The production of bellows through silicone casting would likely result in increased durability under changing loads. However, it has been shown that the assembly technique presented here cannot be applied with silicone, as the photopolymer does not form a bond with the silicone. Alternative attempts using silicone adhesive (SIL-POXY™/1) have also failed to achieve a satisfactory bond between an SLA 3D printing material and silicone. A challenge in the context of silicone casting also remains the development of a suitable casting method, preserving the material properties of the silicone while retaining a small-scale component geometry. At that time, the available materials and joining methods were unable to provide a durable solution. Shortly after the experiments, the material Silicone 40A (Formlabs, USA) was introduced, presenting a new perspective for achieving a long-term stable 3D-printed bellows. The material is composed entirely of silicone, allowing for the effective combination of silicone's optimal properties with the versatility of 3D printing. Subsequent studies will be conducted using this material to investigate its long-term stability. It is anticipated that with this material, the bellows will exhibit higher pressure tolerance, thereby allowing for an improved actuator response time. Consequently, conducting longer experiments without material failure is expected to enable more precise position control.

From this work, future research approaches include:

1. Further miniaturization development to achieve a maximum outer diameter of 10 mm
2. Development of integrable and long-term stable bellows
3. Serial connection of multiple actuators to form a snake-like robot
4. Control of the assembled snake robot

**Author Contributions:** Conceptualization, F.S. and M.S.; methodology, F.S.; investigation, F.S. and J.H.; software, F.S. and M.S.; validation, F.S., J.H. and M.S.; writing—original draft preparation, F.S.; writing—review and editing, F.S. and M.S.; visualization, F.S.; supervision, J.S.; project administration, M.S.; funding acquisition, J.S. All authors have read and agreed to the published version of the manuscript.

**Funding:** This research was funded by German Research Foundation (Deutsche Forschungsgemeinschaft DFG) under the grant number 433586601.

**Data Availability Statement:** No new data were created or analyzed in this study. Data sharing is not applicable to this article.

**Conflicts of Interest:** The authors declare no conflicts of interest.

## References

1. Fatikow, S. *Mikroroboter und Mikromontage: Aufbau, Steuerung und Planung von flexiblen mikroroboterbasierten Montagestationen*, softcover reprint of the hardcover 1st edition 2000 ed.; B.G. Teubner: Stuttgart and Leipzig, 2000.
2. Janocha, H. *Unkonventionelle Aktoren*; Oldenbourg Verlag, 2010. doi:10.1524/9783486711455.
3. Siegfarth, M. Hydraulic miniature actuators controlled by electrorheological fluid. *ACTUATOR 2018 - 16th International Conference and Exhibition on New Actuators and Drive Systems, Conference Proceedings* **2018**.
4. Liljebäck, P. *Snake Robots: Modelling, Mechatronics, and Control*, 1st ed. ed.; Advances in Industrial Control Ser, Springer London Limited: London, 2013.

5. Lee, C.; Kim, M.; Kim, Y.J.; Hong, N.; Ryu, S.; Kim, H.J.; Kim, S. Soft robot review. *International Journal of Control, Automation and Systems* **2017**, *15*, 3–15. doi:10.1007/s12555-016-0462-3.
6. Elhawary, H.; Zivanovic, A.; Davies, B.; Lampérth, M. A review of magnetic resonance imaging compatible manipulators in surgery. *Proceedings of the Institution of Mechanical Engineers. Part H, Journal of engineering in medicine* **2006**, *220*, 413–424. doi:10.1243/09544119JEIM73.
7. Bailly, Y.; Amirat, Y.; Fried, G. Modeling and Control of a Continuum Style Microrobot for Endovascular Surgery. *IEEE Transactions on Robotics* **2011**, *27*, 1024–1030. doi:10.1109/TRO.2011.2151350.
8. Suzumori, K.; Endo, S.; Kanda, T.; Kato, N.; Suzuki, H. A Bending Pneumatic Rubber Actuator Realizing Soft-bodied Manta Swimming Robot. *Proceedings 2007 IEEE International Conference on Robotics and Automation*. IEEE, 2007, pp. 4975–4980. doi:10.1109/ROBOT.2007.364246.
9. Ranzani, T.; Gerboni, G.; Cianchetti, M.; Menciassi, A. A bioinspired soft manipulator for minimally invasive surgery. *Bioinspiration & biomimetics* **2015**, *10*, 035008. doi:10.1088/1748-3190/10/3/035008.
10. Chen, X.; Zhang, X.; Huang, Y.; Cao, L.; Liu, J. A review of soft manipulator research, applications, and opportunities. *Journal of Field Robotics* **2022**, *39*, 281–311. doi:10.1002/rob.22051.
11. Ranzani, T.; Cianchetti, M.; Gerboni, G.; de Falco, I.; Menciassi, A. A Soft Modular Manipulator for Minimally Invasive Surgery: Design and Characterization of a Single Module. *IEEE Transactions on Robotics* **2016**, *32*, 187–200. doi:10.1109/TRO.2015.2507160.
12. Amanov, E.; Nguyen, T.D.; Burgner-Kahrs, J. Tendon-driven continuum robots with extensible sections—A model-based evaluation of path-following motions. *The International Journal of Robotics Research* **2021**, *40*, 7–23. doi:10.1177/0278364919886047.
13. Davidson, J.R.; Krebs, H.I. An Electrorheological Fluid Actuator for Rehabilitation Robotics. *IEEE/ASME Transactions on Mechatronics* **2018**, *23*, 2156–2167. doi:10.1109/TMECH.2018.2869126.
14. J. Furusho, G. Zhang and M. Sakaguchi. Vibration suppression control of robot arms using a homogeneous-type electrorheological fluid.
15. Zatopa, A.; Walker, S.; Menguc, Y. Fully Soft 3D-Printed Electroactive Fluidic Valve for Soft Hydraulic Robots. *Soft robotics* **2018**, *5*, 258–271. doi:10.1089/soro.2017.0019.
16. *IEEE/RSJ International Conference on Intelligent Robots and Systems (IROS), 2012: 7 - 12 Oct. 2012, Vilamoura, Algarve, Portugal*; IEEE: Piscataway, NJ, 2012.
17. Helios Klinikum Aue. Ablauf einer Magenspiegelung - Gastroskopie. <https://www.helios-gesundheit.de/kliniken/ae/unsere-angebote/unsere-fachbereiche/gastroenterologie-hepatologie/patientenwissen-ablauf-gastroskopie/>, accessed on 14.08.2023.
18. HUBS. Auswahl des richtigen 3D-Druckverfahrens: Entscheidungshilfen und allgemeine Richtlinien, die Sie bei der Auswahl des richtigen 3D-Druckverfahrens für Ihre Anwendung unterstützen., 2023.
19. formlabs. Wie Sie den richtigen 3D-Industriedrucker auswählen. <https://formlabs.com/de/blog/industrielle-3d-drucker/>, accessed on 05.09.2023.
20. fomlabs. Elastic Resin: Ein widerstandsfähiges, weiches und flexibles 3D-Druckmaterial. <https://formlabs.com/de/blog/elastic-resin-silikon-3d-druck/>.
21. KG Rubberpoint. Roh- & Zusatzstoffe.
22. 3M. Klebstoff- und Klebebandlösungen: Oberflächenenergie kategorisieren. [https://www.3mdeutschland.de/3M/de\\_DE/kleben-und-verbinden/schulung-weiterbildung/die-wissenschaft-des-klebens/oberflaechenenergie-kategorisieren/](https://www.3mdeutschland.de/3M/de_DE/kleben-und-verbinden/schulung-weiterbildung/die-wissenschaft-des-klebens/oberflaechenenergie-kategorisieren/), accessed on 06.09.2023.
23. Su, H.; Kwok, K.W.; Cleary, K.; Iordachita, I.; Cavusoglu, M.C.; Desai, J.P.; Fischer, G.S. State of the Art and Future Opportunities in MRI-Guided Robot-Assisted Surgery and Interventions. *Proceedings of the IEEE. Institute of Electrical and Electronics Engineers* **2022**, *110*, 968–992. doi:10.1109/JPROC.2022.3169146.
24. Frishman, S.; Kight, A.; Pirozzi, I.; Coffey, M.C.; Daniel, B.L.; Cutkosky, M.R. Enabling In-Bore MRI-Guided Biopsies With Force Feedback. *IEEE transactions on haptics* **2020**, *13*, 159–166. doi:10.1109/TOH.2020.2967375.

**Disclaimer/Publisher's Note:** The statements, opinions and data contained in all publications are solely those of the individual author(s) and contributor(s) and not of MDPI and/or the editor(s). MDPI and/or the editor(s) disclaim responsibility for any injury to people or property resulting from any ideas, methods, instructions or products referred to in the content.